HHS Public Access

Author manuscript

Cytotherapy. Author manuscript; available in PMC 2021 July 25.

Published in final edited form as:

Cytotherapy. 2021 February ; 23(2): 165–175. doi:10.1016/j.jcyt.2020.08.012.

Ex vivo-expanded highly pure ABCB5+ mesenchymal stromal cells as Good Manufacturing Practice-compliant autologous advanced therapy medicinal product for clinical use: process validation and first in-human data

Andreas Kerstan[1,†], **Elke Niebergall-Roth**[2,†], **Jasmina Esterlechner**[2,†], **Hannes M. Schröder**[2], **Martin Gasser**[3], **Ana M. Waaga-Gasser**[3,4], **Matthias Goebeler**[1], **Katrin Rak**[1], **Philipp Schrüfer**[1], **Sabrina Endres**[1], **Petra Hagenbusch**[1], **Korinna Kraft**[5], **Kathrin Dieter**[5], **Seda Ballikaya**[2], **Nicole Stemler**[2], **Samar Sadeghi**[2], **Nils Tappenbeck**[5], **George F. Murphy**[6], **Dennis P. Orgill**[7], **Natasha Y. Frank**[8,9,10,11], **Christoph Ganss**[2,5], **Karin Scharffetter-Kochanek**[12], **Markus H. Frank**[6,10,11,13,‡], **Mark A. Kluth**[2,5,‡,*]

[1]Department of Dermatology, Venereology, and Allergology, University Hospital Würzburg, Würzburg, Germany

[2]TICEBA GmbH, Heidelberg, Germany

[3]Department of Surgery, University Hospital Würzburg, Würzburg, Germany

[4]Renal Division, Brigham and Women's Hospital, Harvard Medical School, Boston, Massachusetts, USA

[5]RHEACELL GmbH & Co. KG, Heidelberg, Germany

[6]Department of Dermatology, Brigham and Women's Hospital, Harvard Medical School, Boston, Massachusetts, USA

[7]Division of Plastic Surgery, Brigham and Women's Hospital, Harvard Medical School, Boston, Massachusetts, USA

[8]Department of Medicine, VA Boston Healthcare System, Boston, Massachusetts, USA

*Correspondence: Mark A. Kluth, PhD, TICEBA GmbH, Im Neuenheimer Feld 517, 69120 Heidelberg, Germany. andreas.kluth@ticeba.com (M.A. Kluth).

†These authors contributed equally to this work and share first authorship.

‡These authors contributed equally to this work and share senior authorship.

Author Contributions

Conception and design of the study: AK, JE, HMS, MGa, SB, NS, SS, GFM, DPO, NYF, CG, MHF and MAK. Acquisition of data: AK, KR, PS, SE, PH, SB, NS and SS. Analysis and interpretation of data: AK, EN-R, JE, HMS, AMW-G, MGo, KK, KD, NT, KS-K and MAK. Drafting or revising the manuscript: AK, EN-R, JE, HMS, MGa, AMW-G, MG, KR, PS, SE, PH, KK, KD, SB, NS, SS, NT, GFM, DPO, NYF, CG, KS-K, MHF and MAK. All authors have approved the final article.

Declaration of Competing Interest

MHF and NYF are inventors or co-inventors of US and international patents assigned to Brigham and Women's Hospital and/or Boston Children's Hospital, Boston, Massachusetts, USA, licensed to TICEBA GmbH, Heidelberg, Germany, and RHEACELL GmbH & Co. KG, Heidelberg, Germany. MHF and KS-K serve as scientific advisors to TICEBA and RHEACELL and participate in corporate-sponsored research collaborations with RHEACELL. EN-R, JE, HMS, SB, NS and SS are employees of TICEBA. KK, KD and NT are employees of RHEACELL. CG is chief executive officer and MAK chief scientific officer of TICEBA and RHEACELL.

Supplementary materials

Supplementary material associated with this article can be found in the online version at doi:10.1016/j.jcyt.2020.08.012.

[9]Division of Genetics, Brigham and Women's Hospital, Harvard Medical School, Boston, Massachusetts, USA

[10]Transplant Research Program, Boston Children's Hospital, Harvard Medical School, Boston, Massachusetts, USA

[11]Harvard Stem Cell Institute, Harvard University, Cambridge, Massachusetts, USA

[12]Department of Dermatology and Allergic Diseases, University Hospital, Ulm, Germany

[13]School of Medical and Health Sciences, Edith Cowan University, Perth, Australia

Abstract

Background aim: Mesenchymal stromal cells (MSCs) hold promise for the treatment of tissue damage and injury. However, MSCs comprise multiple subpopulations with diverse properties, which could explain inconsistent therapeutic outcomes seen among therapeutic attempts. Recently, the adenosine triphosphate-binding cassette transporter ABCB5 has been shown to identify a novel dermal immunomodulatory MSC subpopulation.

Methods: The authors have established a validated Good Manufacturing Practice (GMP)-compliant expansion and manufacturing process by which $ABCB5^+$ MSCs can be isolated from skin tissue and processed to generate a highly functional homogeneous cell population manufactured as an advanced therapy medicinal product (ATMP). This product has been approved by the German competent regulatory authority to be tested in a clinical trial to treat therapy-resistant chronic venous ulcers.

Results: As of now, 12 wounds in nine patients have been treated with 5×10^5 autologous $ABCB5^+$ MSCs per cm^2 wound area, eliciting a median wound size reduction of 63% (range, 32–100%) at 12 weeks and early relief of pain.

Conclusions: The authors describe here their GMP- and European Pharmacopoeia-compliant production and quality control process, report on a pre-clinical dose selection study and present the first in-human results. Together, these data substantiate the idea that $ABCB5^+$ MSCs manufactured as ATMPs could deliver a clinically relevant wound closure strategy for patients with chronic therapy-resistant wounds.

Keywords

ABCB5; advanced therapy medicinal product; chronic wound; GMP manufacturing; mesenchymal stromal cells; venous ulcer

Introduction

Mesenchymal stromal cells (MSCs) are currently the most commonly used non-hematopoietic adult stem cells in regenerative medicine research, providing attractive advantages over other stem cell types. MSCs can be relatively easily isolated from human tissues and expanded *ex vivo*. They can modify the host's immune environment, secrete trophic factors and exhibit a certain trans-differentiation potential [1]. MSCs are being investigated for the treatment of numerous inflammatory, degenerative and autoimmune

diseases [2–10]. In general, MSC-based therapies have appeared feasible, beneficial and safe. Among more than 1400 patients treated in clinical trials with adipose-derived MSCs, very few treatment-related adverse events have been reported [11].

For most potential clinical indications, *ex vivo* cell expansion is required to produce sufficient and scalable cell numbers. However, MSC expansion poses several challenges. Prolonged culture can result in various changes, including morphological abnormalities, attenuated expression of specific surface markers, reduced proliferation, replicative senescence and shifting differentiation potential [12]. Gene expression signatures and functionality can be considerably altered by parameters such as media supplements, culture conditions or culture duration [13]. Since both therapeutic success and patient safety will strongly depend on reliable quality and homogeneity of the expanded cells, the establishment of validated, continuously controlled procedures that comply with the principles of Good Manufacturing Practice (GMP) for safe and reproducible isolation and expansion of MSCs at a clinical-grade level is crucial [14].

The adenosine triphosphate-binding cassette transporter ABCB5 [15] specifically marks a dermal immunomodulatory MSC subpopulation [16,17]. Skin-derived ABCB5$^+$ MSCs express the minimal set of mesenchymal lineage markers [18] CD90, CD105 and CD73, while lacking hematopoietic lineage markers CD34, CD14, CD20 and CD45, and show significantly increased adipogenic, osteogenic and chondrogenic differentiation potential compared with donor-matched ABCB$^-$ fibroblasts or bone marrow-derived MSCs [19]. Similar to adipose tissue-derived MSCs, ABCB5$^+$ MSCs suppress reactive oxygen species release and extracellular trap formation from activated human peripheral neutrophils [17]. In a mouse model of chronic wounds, ABCB5$^+$ MSCs improved wound healing via IL-1RA-mediated shift of prevailing pro-inflammatory M1 macrophages toward the anti-inflammatory M2 subtype [19]. Against the background of substantial patient burden and socioeconomic impact caused by chronic wounds [20,21], ABCB5$^+$ MSCs represent a promising candidate for cell-based wound therapy.

This stimulated the authors to develop a validated manufacturing process to expand, isolate and manufacture human dermal ABCB5$^+$ MSCs as an advanced therapy medicinal product (ATMP). Recently, the authors presented our pre-clinical *in vivo* data demonstrating the local and systemic safety and tolerability of our product [22]. Here the authors describe our GMP- and European Pharmacopoeia-compliant production and quality control process. Enrichment of ABCB5$^+$ MSCs, which constitute only about 2.5% of the total dermal cell population [19], is achieved in a three-step process involving (i) plastic adherence selection, (ii) culture in a highly efficient MSC-selecting medium and (iii) isolation of the ABCB5$^+$ cells using antibody-based magnetic cell sorting. Furthermore, the authors report on a pre-clinical dose selection study and present the first in-human results in therapy-resistant chronic venous ulcers (CVUs).

Methods

Tissue procurement and processing

Skin sampling occurred in accordance with the German Act on Organ and Tissue Donation, Removal and Transplantation (Transplantationsge-setz). After obtaining written informed donor consent, an elliptical ~3 × 1.5 cm^2 excisional skin biopsy was taken from behind the ear. Donors who were serologically positive for HIV1/2 or had active hepatitis B virus, hepatitis C virus or active syphilis (Clinical Laboratory Improvement Amendments-positive/ *Treponema pallidum* antibodies ≥1:80/fluorescent treponemal antibody IgM/rapid plasma reagin) were excluded. The manufacturing process took place in a European Union GMP grade B clean room facility under laminar air flow (A in B). Biopsy tissue was disinfected using povidone-iodine solution (Braunol and Braunoderm; B. Braun, Melsungen, Germany), washed, dissected and subjected to two-step enzymatic digestion using collagenase (Collagenase NB 6 GMP Grade; Nordmark, Uetersen, Germany), followed by non-animal recombinant trypsin (TrypZean; Sigma-Aldrich, Taufkirchen, Germany). Following filtration and washing/centrifugation, pellets were resuspended in a stem cell-favoring medium.

Cell expansion and isolation

Cells were cultured as unsegregated cell cultures in a stem cell-favoring medium (Ham's F-10 supplemented with fetal calf serum, L-glutamine, fibroblast growth factor 2, HEPES, hydrocortisone, insulin, glucose and phorbol 12-myristate 13-acetate) at 37°C, 3.1% carbon dioxide (CO_2) and 90% humidity. During the first 4–6 days of culture, the medium contained penicillin/streptomycin and amphotericin B. Medium was changed at regular intervals to facilitate depletion of non-adherent cells from the culture. Cells were expanded by serial passaging from a C6 well via T25 and T75 flasks to T175 flasks (see supplementary Figure 1). When ≥70% confluency was reached, cells were harvested using non-animal recombinant trypsin and transferred to the next larger vessel. After seven passages, $ABCB5^+$ MSCs were isolated using magnetic beads (micromer TC1 epoxy; Micromod, Rostock, Germany) coated with a mouse anti-human monoclonal antibody directed against sequence 493508 (RFGAYLIQAGRMTPEG) of ABCB5 extracellular loop three [15] (antibody bulk production: Maine Biotechnology Services, Portland, ME, USA; antibody GMP purification: Bibitec, Bielefeld, Germany; virus depletion and safety evaluation of the antibody according to [23]: Charles River, Erkrath, Germany). After enzymatic (TrypZean) detachment of the beads from the cell surface, the isolated $ABCB5^+$ MSCs were cryopreserved in CryoStor CS10 freeze medium (BioLife Solutions, Bothell, WA, USA) and stored in the vapor phase of liquid nitrogen. The manufacturing process allowed for multiple successive isolation cycles after further subcultivation (up to 16 passages in total). Several in-process controls and release criteria monitored and confirmed the quality of the cell cultures and the isolated cells for each isolated cell batch (see supplementary Figure 1).

Real-time quantitative polymerase chain reaction

For detection of *Cdkn1a* expression (forward, AAGACCATGTG-GACCTGTCA, reverse, TTAGGGCTTCCTCTTGGAGA), RNA was purified using the RNeasy mini kit (Qiagen, Hilden, Germany) and reverse transcribed with the Applied Biosystems high-capacity

complementary DNA reverse transcription kit (Thermo Fisher Scientific). Polymerase chain reaction (PCR) was performed using the Applied Biosystems Power SYBR Green PCR master mix (Thermo Fisher Scientific) in a standard program running in an Applied Biosystems StepOne cycler (Thermo Fisher Scientific). Reactions were repeated in triplicate. Integrity of the amplified products was confirmed by melting curve analysis. Efficiency was measured using serial dilution of complementary DNA. Glyceraldehyde 3-phosphate dehydrogenase served as endogenous control. Quantitation of transcript relative to the calibrator was based on a $2^{-\Delta\Delta CT}$ algorithm.

Cell cycle analysis

Cells (2×10^6) were harvested and fixed with ice-cold 70% (v/v) ethanol (added dropwise while vortexing) for at least 30 min at 4°C. After washing in 0.02% ethylenediaminetetraacetic acid, cells were resuspended in RNase A (Thermo Fisher Scientific) and propidium iodide solution and measured flow cytometrically (BD Accuri C6; BD Biosciences, Heidelberg, Germany) using standard gating strategies.

Estimation of cumulative population doubling and division rate

For each passage, cell divisions per passage were calculated as $n = [\log N \log N_0]/\log_2$ where N is the cell number at harvest and N_0 the cell number at seeding. Cumulative population doubling (CPD) was calculated by adding the number of cell divisions for each passage to the sum of the population doubling values of the previous passages. To calculate the division rate, the number of cell divisions per passage was divided by the interval between two passages.

Karyotyping

Karyotyping by G-bands by trypsin using Giemsa banding was performed by an academic contract laboratory. In total, 54 samples from different donors and cell passages were analyzed visually, covering about 350400 bands in 2632 metaphases.

Gene expression analysis

Total RNA was isolated using an RNeasy kit (Qiagen, Hilden, Germany). Gene expression was analyzed by a specialized laboratory service provider using validated microarray technology (human gene expression 8 × 60K microarray; Agilent Technologies, Santa Clara, CA, USA). Quality and integrity of the total RNA was evaluated using the 2100 Bioanalyzer (Agilent Technologies).

Microarrays were performed on samples from four various passages (out of passages seven to 16) per donor for eight donors. Within each donor, data sets were quantile-normalized and the sets from the three higher passages then compared with the lowest passage. From each of these between passage combinations the median gene ratio (including all genes with an average signal >20 and at least 2-fold differential regulation, i.e., $\log_2 < -1$ or >1) was determined. These values were used to determine the median gene ratio for each delta passage value (i.e., passage number difference) for all donors.

Batch analyses

Batch analyses followed validated GMP-compliant procedures according (where applicable) to the requirements of the European Pharmacopoeia (Table 1).

Microbiological examination

Microbiological examination was performed by a certified academic contract laboratory. Cell suspension samples were diluted in sodium chloride peptone buffer, inoculated in BacT/ALERT BPN (anaerobic) and BacT/ALERT BPA (aerobic) culture bottles (bioMérieux, Nürtingen, Germany), respectively, and incubated in the BacT/ALERT 3D60 (bioMérieux) microbial detection system. After 7 days of incubation, all negative samples were seeded onto solid culture medium.

Mycoplasma testing

Cell suspension samples were spiked with internal control DNA and genomic DNA isolated using the Microsart anchored multiplex PCR extraction kit. Isolated DNA was subjected to quantitative PCR, including positive and negative controls (Microsart ATMP *Mycoplasma* kit), an internal isolation control and 10 colony-forming unit sensitivity standards for *Mycoplasma orale*, *M. fermentans* and *M. pneumoniae* (Minerva Biolabs, Berlin, Germany).

Endotoxin testing

After cell isolation, separation from the antibody-conjugated beads and centrifugation, supernatant was diluted 1:10 with Endosafe (Charles River, Charleston, SC, USA) limulus amebocyte lysate reagent water and transferred into an Endosafe PTS cartridge (0.05 EU/mL), which was loaded into an Endosafe PTS reader.

Determination of cell count and vitality

Propidium iodide solution (1 mg/mL) was added to cell suspension samples to stain dead cells. Measurement was performed flow cytometrically (BD Accuri C6) and cell count and vitality calculated.

Determination of viability, CD90 expression and bead residues

Cell suspension samples were incubated with calcein acetoxymethyl ester (to stain metabolically active cells) and an Alexa Fluor 647-conjugated anti-human CD90 antibody (BioLegend, London, UK). Fluorescence was measured flow cytometrically (BD Accuri C6) and viability and content of $CD90^+$ cells calculated. Using cell-free ABCB5 antibody-conjugated bead solution, a gate for detection of potential microbead residues was defined in the forward scatter/side scatter dot plot, and calcein-negative events in that gate were used to calculate residual beads.

Determination of $ABCB5^+$ cell content

After isolation, but before enzymatic detachment of the microbe-ads (which leads to loss of ABCB5 from the cell surface), the $ABCB5^+$ cell content was determined after incubation with an Alexa Fluor 647-coupled donkey anti-mouse secondary antibody (Thermo Fisher Scientific) targeting the anti-ABCB5 antibody used for cell isolation. To allow for

discrimination between ABCB5$^+$ cells and free bead-antibody complexes, calcein acetoxymethyl ester was added to the cell suspension before incubation. Fluorescence was measured flow cytometrically (BD Accuri C6). By gating only events with high calcein fluorescence (indicative of viable cells), unbound bead-antibody complexes were excluded from the ABCB5$^+$ cell calculation.

Tube formation assay

ABCB5$^+$ MSCs were seeded in stem cell medium in a well of a 24-well plate coated with Geltrex basement membrane matrix (Thermo Fisher Scientific) and incubated for 19–22 h at 37°C and 3.1% CO_2. Tube structures were photographed using an inverted microscope (DM IL light-emitting diode; Leica, Wetzlar, Germany) equipped with a digital camera (DFC320; Leica) at ×40 magnification and the photographs qualitatively analyzed per visual inspection for signs of capillary structure formation. Human umbilical vein endothelial cells (Thermo Fisher Scientific) and human skin melanoma cells (SK-MEL-28; American Type Culture Collection, Manassas, VA, USA) served as positive and negative controls, respectively.

IL-1RA secretion assay

Human monocytic (THP-1) cells (LGC Standards; Wesel, Germany) were differentiated to macrophages by incubation in differentiation medium containing 150 nmol/mL phorbol 12-myristate 13-acetate for 48 h at 37°C and 5% CO_2. In two wells of a 24-well plate, 1×10^5 macrophages were co-cultivated with 2×10^4 ABCB5$^+$ MSCs. In one of the two wells, M1 polarization was achieved by stimulation by adding 50 IU/mL interferon γ (Imukin; Boehringer, Ingelheim, Germany) at the start of the co-cultivation and 50 IU/mL interferon γ and 20 ng/mL lipopolysaccharides from *Escherichia coli* O111:B4 (Sigma-Aldrich) after 24 h. After 48 h, supernatants were collected and analyzed for IL-1RA using a colorimetric sandwich enzyme-linked immunosorbent assay kit (Quantikine; R&D Systems, Abingdon, UK).

Dose selection study

Wound healing model—Animal experiments were performed by a specialized contract research organization, meeting the animal protection requirements defined in EU Directive 2010/63/EU [24] and the German Animal Protection Act. The experimental design was approved by the competent local authority (AZ 55.2–1-54–2532.2–33-13; Regierung Oberbayern, Germany).

Forty-six female NOD.*Cg-Prkdc^{scid}Il2rg^{tm1}*WjI/SzJ (NSG) mice (Charles River Wiga, Sulzfeld, Germany) were injected with 200 mg/kg metamizole for peri-surgery pain relief and anesthetized by isoflurane inhalation to receive two circular dermoepidermal full-thickness wounds set paravertebrally on their backs using a 10-mm biopsy punch. Next, 1.875×10^5 (low dose), 3.75×10^5 (low to mid dose), 7.5×10^5 (mid to high dose) or 1.5×10^6 (high dose) human skin-derived ABCB5$^+$ MSCs (pooled from seven donors) suspended in 40 μL vehicle (lactated Ringer's solution containing 2.5% human serum albumin and 0.4% glucose) were dropped on both wounds (n = 10 mice each). As control, six mice received 40 μL vehicle per wound. Wounds were covered with Tegaderm film dressing (3M, Neuss, Germany) and additionally secured using an elastic adhesive bandage and

Leukoplast. For pain relief, mice received 1 mg/kg meloxicam subcutaneously before and up to 3 days after wound setting.

Animals were followed up for 13 days. The wound healing process was documented by standardized photography using an EOS 450D digital camera (Canon) and ImageJ 1.47 processing and analysis software (National Institutes of Health, Bethesda, MD, USA). Thereafter, animals were killed by CO_2 inhalation and wounds macroscopically evaluated. After fixation in neutral buffered formaldehyde (4%), wounds were embedded in Paraplast for histopathological and immunohistochemical examination.

Histopathology—Hematoxylin and eosin-stained slides were histologically evaluated for wound contraction, neovascularization, collagen deposition, fibroblast proliferation, granulation tissue formation, inflammatory cells, re-epithelialization, necrosis, fibrinogen deposition and hemorrhage. Observations were quantified as grade 1 (minimal), grade 2 (slight), grade 3 (moderate), grade 4 (marked) and grade 5 (massive). Data were recorded and analyzed using PathData 10.1 (Pathology Data Systems, Pratteln, Switzerland).

Immunohistochemistry—Paraffin-embedded sections were immunohistochemically stained using rabbit anti-human/mouse CD31 at 1:50 (ab28364; Abcam), rabbit anti-human CD31 at 1:50 (IHC-00055; Bethyl, Montgomery, TX, USA) and rabbit anti-human/mouse cytokeratin 14 at 1:1000 (PRB-155P; Covance/BioLegend), respectively, following validated multistep labeling protocols. In a prior protocol validation study, the anti-human CD31 primary antibody did not cross-react with mouse tissue, and negative control tissues (using the same protocol without the primary antibodies) did not give any positive signal in human or mouse skin sections. Dako EnVision-HRP rabbit/3,3′-diaminobenzidine (Agilent Technologies) was used as a detection system. For positive control, human and NSG mouse skin sections were stained for each marker. Sections were evaluated using a DMR microscope (Leica) equipped with an Axiocam digital color camera with AxioVision 4.0 software (Carl Zeiss, Jena, Germany). Positivity was quantified as no (−), slight (1+), moderate (2+), strong (3+) and intense (4+).

Statistics—Kruskal-Wallis test was performed, followed by Dunn's multiple comparisons, to compare the mean values between treatment groups. $P < 0.05$ was considered statistically significant.

Clinical trial—First in-human data were collected in an ongoing phase 1/2a clinical trial (NCT02742844) evaluating the efficacy and safety of autologous *in vitro*-expanded ABCB5$^+$ MSCs for treatment of conventionally incurable CVUs. The protocol and all relevant documents were approved by the local ethics committee at the University of Würzburg, Germany (164/15_ff), and the competent German regulatory authority, Paul Ehrlich Institute, Langen, Germany (2527/01). All patients gave written informed consent to participate in the trial.

Adult patients were eligible if they presented with a leg CVU (5–50 cm^2), defined as a therapy-resistant leg ulcer that had failed to improve within 3 months or heal within 12 months of optimal phlebological treatment, diagnosed by Doppler ultrasonography, ankle-

brachial index (0.9–1.3) and physical and dermatological examination. Exclusion criteria were ulcers extending to the underlying muscle, tendon or bone; diabetes mellitus (hemoglobin A1c >7.5%); peripheral artery disease requiring treatment; acute or untreated deep vein thrombosis; ulcer infection; skin disorders or (pre-)cancerous lesions adjacent to the ulcer.

ABCB5$^+$ MSCs were derived from a patient's skin biopsy and expanded as described earlier over 6–20 weeks, depending on the number of subcultivation and ABCB5$^+$ cell isolation cycles required to produce the quantity of cells demanded (as defined by the patient's wound size). Patients whose CVU enlarged >25% or diminished >50% during this period were excluded from efficacy (but not safety) evaluation, ensuring that only those ulcers that had been arrested in a chronic state were evaluated. On the day of treatment (day 0), the wound was debrided under local anesthesia, a suspension containing 1×10^7 ABCB5$^+$ MSCs per 1 mL vehicle dropped onto the wound surface to supply 5×10^5 cells per cm^2 wound area and the wound covered with Tegaderm film dressing. Between day 1 and day 3, the Tegaderm dressing was replaced with a foam dressing—Mepilex (Mölnlycke, Düsseldorf, Germany) or Biatain (Coloplast, Hamburg, Germany)—which was used until week 12. In addition, patients received standard compression dressings. Patients presenting with more than one ulcer were offered to have the other wounds (defined as non-target ulcers) treated, depending on whether therapy of the target ulcer appeared efficacious and safe.

Wound healing was documented by standardized photography (Surface Pro 3 tablet; Microsoft Corporation, Redmond, WA, USA) using PictZar planimetry software (BioVisual Technologies, Elmwood Park, NJ, USA). Primary efficacy endpoint was the percentage of wound size reduction at week 12. Main secondary efficacy endpoints were quantitative and qualitative wound parameters and pain score per visual analog scale (ranging from 0 = no to 10 = worst imaginable pain), which were assessed throughout the 12-week period. Primary safety outcome measure was the occurrence of adverse events throughout the 12 months following treatment.

Results

Characteristics of cultured ABCB5$^+$ MSCs

Cultured ABCB5$^+$ MSCs exhibited typical fibroblast-like spindle-shaped MSC morphology characterized by a small cell body and a few long and thin cell processes (Figure 1A). Cell proliferation, measured by live cell counting over 13 days of culture, slowed down in parallel with increasing cell confluency (Figure 1B). After reaching 100% confluency, live cell count did not increase further, indicating that the cells were arrested in a non-proliferative state. In line with this, messenger RNA expression of *Cdkn1a* (encoding the senescence marker p21) was induced up to 7-fold at 99% confluency (Figure 1C). Cell cycle analysis of 503 batches from 260 donors consistently revealed an expectable phase distribution, with the majority of cells (72.4% ± 8.5%) being in the G1 phase (Figure 1D).

Process validation

Growth behavior—CPD values, division rates and yield of ABCB5$^+$ cells were compared in 15 donors up to 16 passages. CPD values increased linearly with passage number, demonstrating exponential growth (Figure 2A). Mean division rate was approximately 0.35 per day, corresponding to cell doubling about every 3 days (Figure 2B).

Genetic stability—Of 43 samples covering passages three to 16, 32 samples (75%) exhibited an inconspicuous karyotype, eight samples (19%) exhibited an aberrant karyotype (such as mosaic structures, loss of chromosomes or micro-mosaics in singular cells) and three samples (7%) exhibited a pathologic karyotype. In exemplary analyses, those cultures that exhibited an aberrant karyotype in passage five did not show any abnormalities in passage 11, suggesting a trend toward loss of abnormal karyotypes with increasing passage.

Gene expression—Gene expression microarrays were performed on samples from eight donors. Gene expression profiles showed no significant differences between batches from a given donor and between donors (see supplementary Figure 2). Analysis of the gene ratios for each delta passage value (i.e., difference between numbers of two passages that were compared with each other) showed that the gene expression profile did not significantly change with increasing delta value (Figure 2C; also see supplementary Table 1). Analysis of the gene expression ratios at Δ_{max} (i.e., between the two samples with the greatest passage number difference) of all eight donors (42 992 genes per analysis in total) revealed that only 2.4% (range, 0.3–5.2%) of genes were highly differentially (>5-fold) regulated (see supplementary Figure 3A). There was no correlation between the percentage of differentially regulated genes and the delta passage value. In an intra-donor (one of the two donors with the highest Δ_{max} value) analysis of the three delta passages, the percentage of highly differentially regulated genes ranged from 2% to 3% (see supplementary Figure 3B).

ABCB5$^+$ cell content—The percentage of ABCB5$^+$ cells in culture showed a continuous but statistically non-significant decline during the expansion process, from 9.7% at passage seven to 5.3% at passage 16. Mean yield of ABCB5$^+$ MSCs was 26.3×10^6 cells per batch (Figure 2D).

Batch quality control—Batch analyses were performed on 155 cell batches (IL-1RA secretion assay, 75 batches). Overall, >98% of batches fulfilled the release specifications (Table 1).

Dose selection study—Topical application of manufactured human ABCB5$^+$ MSCs in the low- to mid- and high- to mid-dose regimen facilitated closure of punch biopsy wounds in NSG mice, as evidenced by significantly lower mean wound sizes from day 9 on compared with control (Figure 3A–C). The high-dose group was retrospectively excluded from inter-group wound size comparisons since in this group the baseline wound size was significantly lower compared with control. At day 13, about 30% of the wounds in the mid- and high-dose groups had fully healed, in contrast to none of the vehicle-treated and 5% (one out of 18) of the low-dose-treated wounds (Figure 3D). One animal in the low-dose group was euthanized on day 7 due to loss of body weight and poor general condition, which

was attributed to high physical strain caused by the relatively large wounds. No cell treatment-related clinical findings were noted.

Histologically, wound contraction was slightly enhanced in all cell-treated groups versus control ($P < 0.05$ for low to mid dose only). Similarly, cell-treated groups exhibited somewhat greater mean scores for collagen accumulation ($P < 0.05$ for low to mid and high dose) and re-epithelialization (not significant) than control (data not shown). No obvious differences between groups were observed for fibroblast proliferation, inflammatory cells, granulation tissue formation and neovascularization. Occasionally, small focal necroses, exudation of fibrin fibers and hemorrhages were noted in some animals across all groups. Immunohistochemically, the wounds showed a dose-dependent increase in CD31 expression, which was significant for human CD31 but not for unspecific CD31 (as no antibody to specifically detect mouse CD31 was available, the authors had to use an antibody that detected both mouse and human CD31) and cytokeratin 14 expression (Figure 3E–G).

Clinical trial in CVU patients—Thus far, 12 CVUs (nine target and three non-target wounds) in nine patients (three men/six women, median age 77 years [range, 48–83], median body mass index 31 kg/m^2 [range, 25–38]) have been treated with autologous ABCB5$^+$ MSCs. At baseline, the nine target ulcers had persisted between 5 months and 60 years (median, 15 years) and were between 1.8 cm^2 and 45 cm^2 in size. Three target ulcers were excluded from efficacy evaluation because the wounds had shown a healing tendency during the period of *ex vivo* cell expansion; the other six target ulcers were eligible for efficacy evaluation. In these patients, the target wound size decreased with time, achieving a median reduction of 59% (range, 29–84%) at week 6 and 63% (range, 32–100%) at week 12 (Figure 4; also see supplementary Figure 4). This was accompanied by wound quality improvement and early-onset pain relief starting day 1–3 after cell transfer, as reflected by the median visual analog scale pain score dropping from 4 at baseline to 1.5 at week 12. Immunohistochemical analysis of cell debris covering the wound of one patient at day 23 after cell application most likely demonstrated the presence of applied ABCB5$^+$ cells facing the ulcer contact side (see supplementary Figure 5).

During the 12-month safety follow-up, no adverse event related to cell treatment was reported in any patient. One pre-treatment-emergent adverse event related to skin biopsy (pain) occurred.

Discussion

To enable safe, effective and reproducible therapeutic use of human ABCB5$^+$ MSCs, the authors developed and validated a manufacturing and quality control process through which these cells can be derived from human skin biopsies, expanded, isolated and manufactured as a clinical-grade ATMP, guaranteeing reliable cell quality and homogeneity. Cultured ABCB5$^+$ MSCs exhibited normal growth behavior, without any signs of overgrowth potential (Figure 1B–D). CPD values and division rates indicated homogeneous cell expansion during (at least) 16 passages (Figure 2A,B), and passaging did not appear to significantly affect gene expression (Figure 1C). Even though the percentage of ABCB5$^+$

cells showed a certain decrease with higher passage numbers, cell yield was still sufficient at passage 16 (Figure 2D).

A major concern regarding the safety of therapies using *ex vivo*-expanded cells is the risk of genetic changes that may lead to tumorigenic transformation [25,26]. Karyotypic assays covering passages three to 16 detected aberrant karyotypes in 19% and pathologic karyotypes in 7% of analyzed samples. A certain degree of aberrant karyotypes occurring during MSC culture has also been reported by others [27–31]. This was essentially attributed to the artificial growth conditions in two-dimensional culture associated with enhanced cell replication and, consequently, errors in cell division. In addition, the authors cannot rule out whether an aberrant phenotype detected during culture was already present in the donor tissue. In any case, an important question is whether such karyotypic aberrations confer a selective growth advantage [29]. Exemplary analyses suggested a trend toward loss of abnormal MSC karyotypes when the passage number increased further, which has also been described by others [28–31]. These observations have been linked to apoptosis, cell cycle arrest or replicative senescence caused by deleterious DNA alterations [29–31] and might indicate that karyotypic alterations in MSCs during culture are not associated with a selective growth advantage, but rather confer a growth disadvantage to the affected cell [29]. On the functional level, the authors have implemented several in-process controls, including morphology, contact inhibition, time between passages (CPD), cell cycle analysis and detection of possible aneuploidies to identify signals of non-physiological cell behavior during cell expansion. Furthermore, a thorough pre-clinical study program on the *in vivo* safety of the authors' cell product has not revealed any signal for tumorgenicity of *ex vivo*-expanded ABCB5$^+$ MSCs [22].

Comparative gene expression analysis, revealing only rare variations between different passages of a given donor and between donors, indicated intra- and inter-donor homogeneity (Figure 2D; also see supplementary Figure 3). These findings suggest that the authors' manufacturing process does not induce significant alterations in the gene expression profile of ABCB5$^+$ MSCs during passaging.

Before being released, each batch of ABCB5$^+$ MSCs undergoes a series of tests to verify its conformity with pre-specified criteria (Table 1). Overall, >98% of 155 batches produced thus far have fulfilled the specifications. Batch testing includes two potency (functionality) assays to test for endothelial differentiation ability (tube formation assay) and immunomodulatory properties (IL-1RA secretion assay). So far, no robust data exist that would allow quantitative correlation of the amount of secreted IL-1RA with the magnitude of the clinical effect. For this reason, in routine batch analysis, the authors monitor whether the batch exceeds a minimal secretion level of 125 mg/mL IL-1RA to basically demonstrate biologically active cells.

To select a starting dose for first in-human use of the manufactured ABCB5$^+$ MSC product, a Good Laboratory Practice study was carried out in a mouse wound healing model. In this study, treatment with 3.75×10^5 cells per wound or higher accelerated wound healing (Figure 3A–D). Increases in cytokeratin 14 and CD31 expression in the wound tissue indicated increased accumulation of epithelial and endothelial cells, respectively, after

treatment with human ABCB5$^+$ MSCs (Figure 3E–G). It is noteworthy that enhanced CD31 expression was, to a great extent, attributable to an increase in human-specific CD31 positivity. This observation suggests that a portion of the grafted cells had trans-differentiated to the endothelial lineage, which is supported by several reports of other authors on *in vivo* endothelial trans-differentiation of transplanted MSCs [32–37].

The lowest cell dose at which acceleration of wound healing was observed in the mouse model (i.e., 3.75×10^5 cells per wound) roughly corresponded to 5×10^5 cells/cm^2 wound surface area, which was set as the starting dose for first in-human use. In the clinical trial, a maximum baseline wound size of 50 cm^2 (to guarantee the required cell quantity was supplied) was defined. This translates into a maximum per-patient cell load of 2.5×10^7 cells, corresponding to a maximum cell dose of 4.2×10^5 MSCs per kg (assuming 60 kg body weight). This dose is nearly 800 times below the subcutaneous no-observed-adverse-effect level (as recommended by the US Department of Health and Human Services [38]) of 3.33×10^8 ABCB5$^+$ MSCs per kg previously determined in a pre-clinical Good Laboratory Practice study on repeated-dose toxicity [22].

The authors' first in-human data suggest that cell therapy facilitated tissue repair of CVUs that had not adequately responded to prior guideline-adherent standard (compression) therapy [39–42]. Under pre-defined conditions, excluding those ulcers from efficacy evaluation that showed a healing tendency during the period of *ex vivo* cell expansion, topical application of 5×10^5 ABCB5$^+$ MSCs per cm^2 wound area elicited a median wound size reduction of 63% (range, 32100%) within 12 weeks. The absence of any treatment-related adverse event in all patients confirmed good tolerability and overall safety of therapy.

It is noteworthy that wound healing rate was greatest until week 6 (Figure 4B, red shaded area), slowing down thereafter, even if a certain portion of this outcome can be attributed to an increase in the wound of patient 8 coinciding with changes in routine wound care (Figure 4B). These findings support the idea that the initial impact of ABCB5$^+$ MSCs on chronic wounds predominantly relies on transient, immunomodulatory effects rather than on longer-lasting processes such as engraftment and (trans-)differentiation. Indeed, chronic wounds such as non-healing CVUs typically fail to progress through the normal pattern of wound repair (i.e., hemostasis, inflammation, proliferation and remodeling), remaining instead in a chronic inflammatory state characterized by unrestrained accumulation of activated pro-inflammatory M1 macrophages [43]. By releasing IL-1RA, ABCB5$^+$ MSCs have been shown to shift the prevalence of M1 macrophages in chronic wounds toward repair-promoting anti-inflammatory M2 macrophages, thus helping the wound overcome its chronic inflammatory state [19]. Conceivably, once the wound has left the state of chronic inflammation and entered the physiological pattern of wound repair, the wound may benefit from further modes of action of MSCs, such as trans-differentiation into endothelial cells required for blood vessel formation, as observed in the dose selection study (Figure 3E,F) and phenotypically demonstrated by the tube formation assay, and paracrine secretion of proangiogenic growth factors, as has been described for various MSC types in the literature [44–46]. Thus, a second application of ABCB5$^+$ MSCs after the initial beneficial effect has tapered off might be capable of resuming the healing process to finally lead to complete wound closure.

Mainly due to the nature of our ATMP, the present clinical trial comes with some limitations. First, the number of treated patients is small, owing to the labor- and time-consuming manufacturing process, which, in the autologous setting, must be carried out for each patient individually. Second, the authors could not include a control group, as placebo treatment would not ethically justify a sham biopsy to mimic MSC isolation. Third, wound size at screening needed to be limited to 50 cm^2 to guarantee the required cell quantity was supplied in every case. All these limitations could potentially be overcome by using allogeneic $ABCB5^+$ MSCs, which could be manufactured as a readily available off-the-shelf product. This is considered feasible given that the low immunogenicity and the immunomodulatory properties of culture-expanded MSCs contribute to a diminished immune response to allogeneic MSCs [47–50]. Moreover, pre-clinical and clinical trials directly comparing the safety and therapeutic efficacy of autologous and allogeneic MSCs have revealed similar outcomes [51] or even a greater efficacy of allogeneic cells [16,52]. As a result, the authors are currently testing $ABCB5^+$ MSCs in the allogeneic setting in two ongoing clinical trials in patients with CVUs (NCT03257098) and diabetic foot ulcers (NCT03267784).

It is worth noting that it is not only patients suffering from local inflammatory conditions who may benefit from $ABCB5^+$ MSC therapy. The substantial anti-inflammatory potential of $ABCB5^+$ MSCs and their convincing safety profile make our ATMP a promising candidate for intravenous treatment of systemic inflammatory conditions as well. Thus far, significant benefit delivered by human $ABCB5^+$ MSCs in pre-clinical models of epidermolysis bullosa [53] and liver disease [54] has stimulated further clinical trials of allogeneic $ABCB5^+$ MSCs in recessive dystrophic epidermolysis bullosa (NCT03529877) and acute-on-chronic liver failure (NCT03860155).

Supplementary Material

Refer to Web version on PubMed Central for supplementary material.

Acknowledgments

The authors thank the Section of Medical Microbiology and Hygiene (Prof. Dr. med. Klaus Heeg, head) at the Center of Infectious Diseases, Heidelberg University Hospital, Heidelberg, Germany, for the microbiological examinations; the Institute of Human Genetics (Prof. Dr. med. Christian Schaaf, head), Heidelberg University Hospital, for karyotyping; OakLabs GmbH, Hennigsdorf, Germany, for the gene expression analyses; Aurigon Life Science GmbH, Tutzing, Germany, for conducting the animal study; and FGK Clinical Research GmbH, Munich, Germany, for expert support in the clinical trial.

Funding

No funding was received.

References

[1]. Menaa F, Shahrokhi S, Prasad Shastri V. Impact and challenges of mesenchymal stem cells in medicine: an overview of the current knowledge. Stem Cells Int 2018;2018:5023925.

[2]. Yun CW, Lee SH. Enhancement of functionality and therapeutic efficacy of cell-based therapy using mesenchymal stem cells for cardiovascular disease. Int J Mol Sci 2019;20:982.

[3]. Zhao L, Chen S, Yang P, Cao H, Li L. The role of mesenchymal stem cells in hematopoietic stem cell transplantation: prevention and treatment of graft-versus-host disease. Stem Cell Res Ther 2019;10:182. [PubMed: 31227011]

[4]. Wang M, Yuan Q, Xie L. Mesenchymal stem cell-based immunomodulation: properties and clinical application. Stem Cells Int 2018;2018:3057624.

[5]. Mukai T, Tojo A, Nagamura-Inoue T. Mesenchymal stromal cells as a potential therapeutic for neurological disorders. Regen Ther 2018;9:32–7. [PubMed: 30525073]

[6]. Cho J, D'Antuono M, Glicksman M, Wang J, Jonklaas J. A review of clinical trials: mesenchymal stem cell transplant therapy in type 1 and type 2 diabetes mellitus. Am J Stem Cells 2018;7:82–93. [PubMed: 30510843]

[7]. de Miguel MP, Prieto I, Moratilla A, Arias J, Aller MA. Mesenchymal stem cells for liver regeneration in liver failure: from experimental models to clinical trials. Stem Cells Int 2019;2019:3945672.

[8]. Bochon B, Kozubska M, Surygala G, Witkowska A, Kuzniewicz R, Grzeszczak W, et al. Mesenchymal stem cells—potential applications in kidney diseases. Int J Mol Sci 2019;20:2462.

[9]. Fan XL, Zhang Z, Ma CY, Fu QL. Mesenchymal stem cells for inflammatory airway disorders: promises and challenges. Biosci Rep 2019;39:20182160.

[10]. Rivera-Izquierdo M, Cabeza L, Lainez-Ramos-Bossini A, Quesada R, Perazzoli G, Alvarez P, et al. An updated review of adipose-derived mesenchymal stem cells and their applications in musculoskeletal disorders. Expert Opin Biol Ther 2019;19:233–48. [PubMed: 30653367]

[11]. Toyserkani NM, Jorgensen MG, Tabatabaeifar S, Jensen CH, Sheikh SP, Sorensen JA. Concise review: a safety assessment of adipose-derived cell therapy in clinical trials: a systematic review of reported adverse events. Stem Cells Transl Med 2017;6:1786–94. [PubMed: 28722289]

[12]. Wagner W, Horn P, Castoldi M, Diehlmann A, Bork S, Saffrich R, et al. Replicative senescence of mesenchymal stem cells: a continuous and organized process. PLoS One 2008;3:e2213.

[13]. Liu S, de Castro LF, Jin P, Civini S, Ren J, Reems JA, et al. Manufacturing differences affect human bone marrow stromal cell characteristics and function: comparison of production methods and products from multiple centers. Sci Rep 2017;7:46731. [PubMed: 28447618]

[14]. Torre ML, Lucarelli E, Guidi S, Ferrari M, Alessandri G, De Girolamo L, et al. Ex vivo expanded mesenchymal stromal cell minimal quality requirements for clinical application. Stem Cells Dev 2015;24:677–85. [PubMed: 25517941]

[15]. Frank NY, Pendse SS, Lapchak PH, Margaryan A, Shlain D, Doeing C, et al. Regulation of progenitor cell fusion by ABCB5 P-glycoprotein, a novel human ATP-binding cassette transporter. J Biol Chem 2003;278:47156–65. [PubMed: 12960149]

[16]. Schatton T, Yang J, Kleffel S, Uehara M, Barthel SR, Schlapbach C, et al. ABCB5 identifies immunoregulatory dermal cells. Cell Rep 2015;12:1564–74. [PubMed: 26321644]

[17]. Jiang D, Muschhammer J, Qi Y, Kugler A, de Vries JC, Saffarzadeh M, et al. Suppression of neutrophil-mediated tissue damage—a novel skill of mesenchymal stem cells. Stem Cells 2016;34:2393–406. [PubMed: 27299700]

[18]. Dominici M, Le Blanc K, Mueller I, Slaper-Cortenbach I, Marini F, Krause D, et al. Minimal criteria for defining multipotent mesenchymal stromal cells. The International Society for Cellular Therapy position statement. Cytotherapy 2006;8: 315–7. [PubMed: 16923606]

[19]. Vander Beken S, de Vries JC, Meier-Schiesser B, Meyer P, Jiang D, Sindrilaru A, et al. Newly defined ATP-binding cassette subfamily B member 5 positive dermal mesenchymal stem cells promote healing of chronic iron-overload wounds via secretion of interleukin-1 receptor antagonist. Stem Cells 2019;37:1057–74. [PubMed: 31002437]

[20]. Hu MS, Borrelli MR, Lorenz HP, Longaker MT, Wan DC. Mesenchymal stromal cells and cutaneous wound healing: a comprehensive review of the background, role, and therapeutic potential. Stem Cells Int 2018;2018:6901983.

[21]. Ojeh N, Pastar I, Tomic-Canic M, Stojadinovic O. Stem cells in skin regeneration, wound healing, and their clinical applications. Int J Mol Sci 2015;16:25476–501. [PubMed: 26512657]

[22]. Tappenbeck N, Schröder HM, Niebergall-Roth E, Hassinger F, Dehio U, Dieter K, et al. In vivo safety profile and biodistribution of GMP-manufactured human skin-derived ABCB5-positive

mesenchymal stromal cells for use in clinical trials. Cytotherapy 2019;21:546–60. [PubMed: 30878384]

[23]. International Conference on Harmonization of Technical Requirements for Registration of Pharmaceuticals for Human Use. In: ICH Harmonised Tripartite Guideline Q5A(R1): Viral safety evaluation of biotechnology products derived from cell lines of human or animal origin; 1999. https://ichguideline.weebly.com/uploads/2/6/2/1/26210522/q5a_r1__step4.pdf [accessed 4 May, 2020].

[24]. Parliament European and Council of the European Union. Directive 2010/63/EU of the European Parliament and of the Council of 22 September 2010 on the protection of animals used for scientific purposes. Official Journal of the European Union 2010;L276:33–79.

[25]. Miura M, Miura Y, Padilla-Nash HM, Molinolo AA, Fu B, Patel V, et al. Accumulated chromosomal instability in murine bone marrow mesenchymal stem cells leads to malignant transformation. Stem Cells 2006;24:1095–103. [PubMed: 16282438]

[26]. Rosland GV, Svendsen A, Torsvik A, Sobala E, McCormack E, Immervoll H, et al. Long-term cultures of bone marrow-derived human mesenchymal stem cells frequently undergo spontaneous malignant transformation. Cancer Res 2009;69: 5331–9. [PubMed: 19509230]

[27]. Wang Y, Zhang Z, Chi Y, Zhang Q, Xu F, Yang Z, et al. Long-term cultured mesenchymal stem cells frequently develop genomic mutations but do not undergo malignant transformation. Cell Death Dis 2013;4:e950.

[28]. Ueyama H, Horibe T, Hinotsu S, Tanaka T, Inoue T, Urushihara H, et al. Chromosomal variability of human mesenchymal stem cells cultured under hypoxic conditions. Journal Cell Mol Med 2012;16:72–82. [PubMed: 21418515]

[29]. Tarte K, Gaillard J, Lataillade JJ, Fouillard L, Becker M, Mossafa H, et al. Clinical-grade production of human mesenchymal stromal cells: occurrence of aneuploidy without transformation. Blood 2010;115:1549–53. [PubMed: 20032501]

[30]. Binato R, de Souza Fernandez T, Lazzarotto-Silva C, Du Rocher B, Mencalha A, Pizzatti L, et al. Stability of human mesenchymal stem cells during in vitro culture: considerations for cell therapy. Cell Prolif 2013;46:10–22. [PubMed: 23163975]

[31]. Stultz BG, McGinnis K, Thompson EE, Lo Surdo JL, Bauer SR, Hursh DA. Chromosomal stability of mesenchymal stromal cells during in vitro culture. Cytotherapy 2016;18:336–43. [PubMed: 26780865]

[32]. Ben Menachem-Zidon O, Gropp M, Ben Shushan E, Reubinoff B, Shveiky D. Systemically transplanted mesenchymal stem cells induce vascular-like structure formation in a rat model of vaginal injury. PLoS One 2019;14:e0218081. [PubMed: 31194823]

[33]. Chen J, Park HC, Addabbo F, Ni J, Pelger E, Li H, et al. Kidney-derived mesenchymal stem cells contribute to vasculogenesis, angiogenesis and endothelial repair. Kidney Int 2008;74:879–89. [PubMed: 18596729]

[34]. Yue WM, Liu W, Bi YW, He XP, Sun WY, Pang XY, et al. Mesenchymal stem cells differentiate into an endothelial phenotype, reduce neointimal formation, and enhance endothelial function in a rat vein grafting model. Stem Cells Dev 2008;17:785–93. [PubMed: 18522495]

[35]. Hu X, Yu SP, Fraser JL, Lu Z, Ogle ME, Wang JA, et al. Transplantation of hypoxia-preconditioned mesenchymal stem cells improves infarcted heart function via enhanced survival of implanted cells and angiogenesis. J Thorac Cardiovasc Surg 2008;135:799–808. [PubMed: 18374759]

[36]. Song YS, Lee HJ, Park IH, Kim WK, KU JH, Kim SU. Potential differentiation of human mesenchymal stem cell transplanted in rat corpus cavernosum toward endothelial or smooth muscle cells. Int J Impot Res 2007;19:378–85. [PubMed: 17460699]

[37]. Fu X, Fang L, Li X, Cheng B, Sheng Z. Enhanced wound-healing quality with bone marrow mesenchymal stem cells autografting after skin injury. Wound Repair Regen 2006;14:325–35. [PubMed: 16808812]

[38]. U.S. Department of Health and Human Services. In: Food and Drug Administration. Guidance for Industry: Chronic Cutaneous Ulcer and Burn Wounds—Developing Products for Treatment; 2006. https://www.fda.gov/media/71278/download [accessed 31 July, 2020].

[39]. O'Donnell TF Jr., Passman MA, Marston WA, Ennis WJ, Dalsing M, Kistner RL, et al. Management of venous leg ulcers: clinical practice guidelines of the Society for Vascular Surgery and the American Venous Forum. J Vasc Surg 2014;60(suppl 2):3S–59S. [PubMed: 24974070]

[40]. Franks PJ, Barker J, Collier M, Gethin G, Haesler E, Jawien A, et al. Management of patients with venous leg ulcers: challenges and current best practice. J Wound Care 2016;25(suppl 6):S1–67.

[41]. European Dermatology Forum. Evidence-based (S3) guidelines for diagnostics and treatment of venous leg ulcers. J Eur Acad Dermatol Venereol 2016;30:1843–75. [PubMed: 27558268]

[42]. Marston W, Tang J, Kirsner RS, Ennis W. Wound Healing Society 2015 update on guidelines for venous ulcers. Wound Repair Regen 2016;24:136–44. [PubMed: 26663616]

[43]. Sindrilaru A, Peters T, Wieschalka S, Baican C, Baican A, Peter H, et al. An unrestrained proinflammatory M1 macrophage population induced by iron impairs wound healing in humans and mice. J Clin Invest 2011;121:985–97. [PubMed: 21317534]

[44]. An Y, Liu WJ, Xue P, Ma Y, Zhang LQ, Zhu B, et al. Autophagy promotes MSC-mediated vascularization in cutaneous wound healing via regulation of VEGF secretion. Cell Death Dis 2018;9:58. [PubMed: 29352190]

[45]. Tao H, Han Z, Han ZC, Li Z. Proangiogenic features of mesenchymal stem cells and their therapeutic applications. Stem Cells Int 2016;2016:1314709.

[46]. Ge Q, Zhang H, Hou J, Wan L, Cheng W, Wang X, et al. VEGF secreted by mesenchymal stem cells mediates the differentiation of endothelial progenitor cells into endothelial cells via paracrine mechanisms. Mol Med Rep 2018;17:1667–75. [PubMed: 29138837]

[47]. Le Blanc K, Tammik C, Rosendahl K, Zetterberg E, Ringden O. HLA expression and immunologic properties of differentiated and undifferentiated mesenchymal stem cells. Exp Hematol 2003;31:890–6. [PubMed: 14550804]

[48]. Klyushnenkova E, Mosca JD, Zernetkina V, Majumdar MK, Beggs KJ, Simonetti DW, et al. T cell responses to allogeneic human mesenchymal stem cells: immunogenicity, tolerance, and suppression. J Biomed Sci 2005;12: 47–57. [PubMed: 15864738]

[49]. Ankrum JA, Ong JF, Karp JM. Mesenchymal stem cells: immune evasive, not immune privileged. Nat Biotechnol 2014;32:252–60. [PubMed: 24561556]

[50]. Berglund AK, Fortier LA, Antczak DF, Schnabel LV. Immunoprivileged no more: measuring the immunogenicity of allogeneic adult mesenchymal stem cells. Stem Cell Res Ther 2017;8:288. [PubMed: 29273086]

[51]. Hare JM, Fishman JE, Gerstenblith G, DiFede Velazquez DL, Zambrano JP, Suncion VY, et al. Comparison of allogeneic vs autologous bone marrow-derived mesenchymal stem cells delivered by transendocardial injection in patients with ischemic cardiomyopathy: the POSEIDON randomized trial. JAMA 2012;308:2369–79. [PubMed: 23117550]

[52]. Premer C, Blum A, Bellio MA, Schulman IH, Hurwitz BE, Parker M, et al. Allogeneic mesenchymal stem cells restore endothelial function in heart failure by stimulating endothelial progenitor cells. EBioMedicine 2015;2:467–75. [PubMed: 26137590]

[53]. Webber BR, O'Connor KT, McElmurry RT, Durgin EN, Eide CR, Lees CJ, et al. Rapid generation of Col7a1$^{-/-}$ mouse model of recessive dystrophic epidermolysis bullosa and partial rescue via immunosuppressive dermal mesenchymal stem cells. Lab Invest 2017;97:1218–24. [PubMed: 28892093]

[54]. Hartwig V, Dewidar B, Lin T, Dropmann A, Ganss C, Kluth MA, et al. Human skin-derived ABCB5^{+} stem cell injection improves liver disease parameters in Mdr2KO mice. Arch Toxicol 2019;93:2645–60. [PubMed: 31435712]

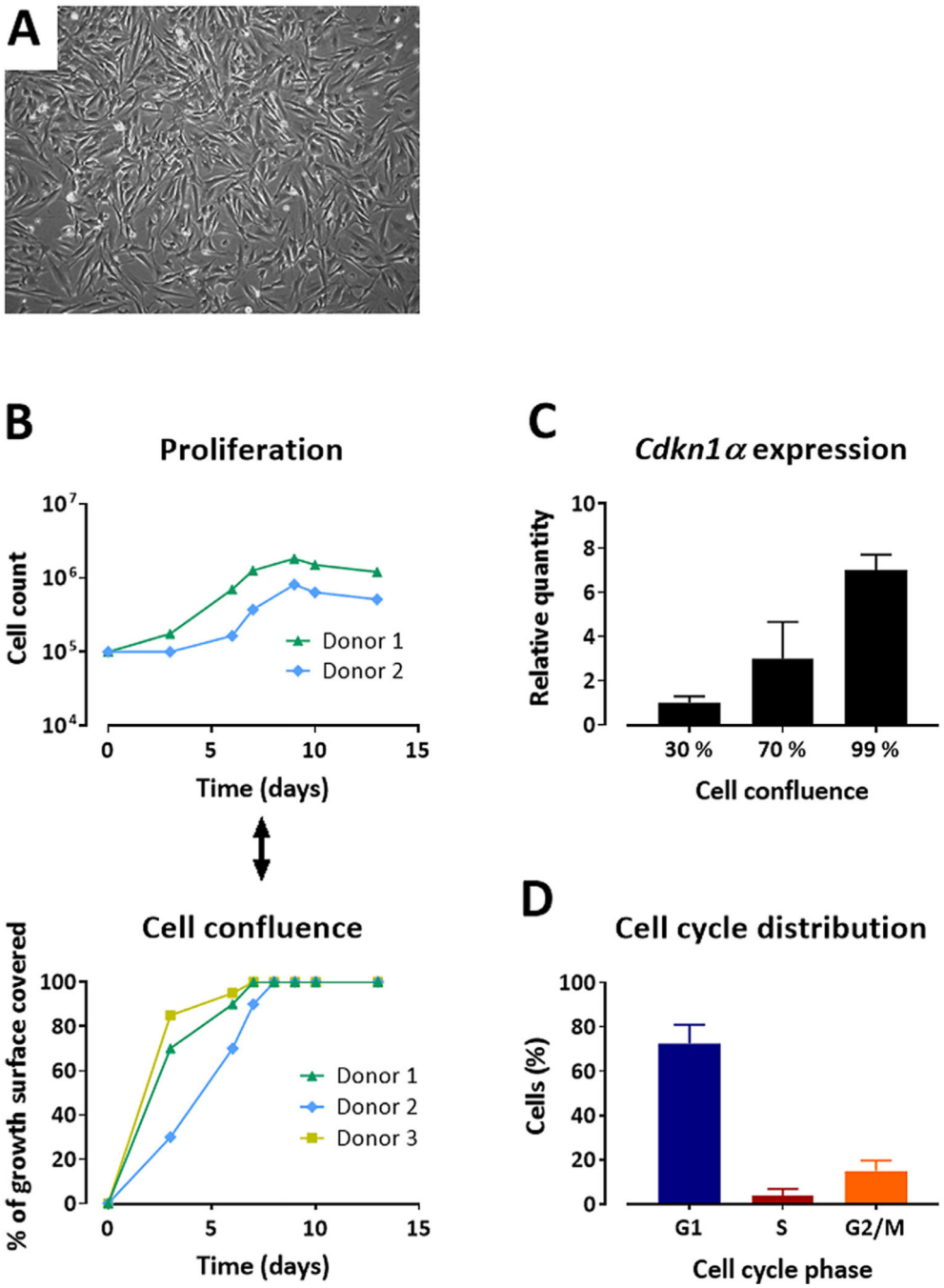

Figure 1.

Morphology and growth behavior of cultured ABCB5$^+$ MSCs. (A) Cultured MSCs at about 80% confluency, displaying a spindled-shaped appearance. Magnification ×200. (B) Live cell count measured over time (upper panel) in parallel with cell confluency as determined visually (lower panel) from representative donors. (C) *Cdkn1α* gene expression (means of relative quantification + SD) was determined at 30%, 70% and 99% confluency. (D) Cell cycle phase distribution expressed as mean (± SD) percentage of cells in G1, S and G2/M

phases; n = 503 batches from 260 donors. SD, standard deviation. (Color version of figure is available online).

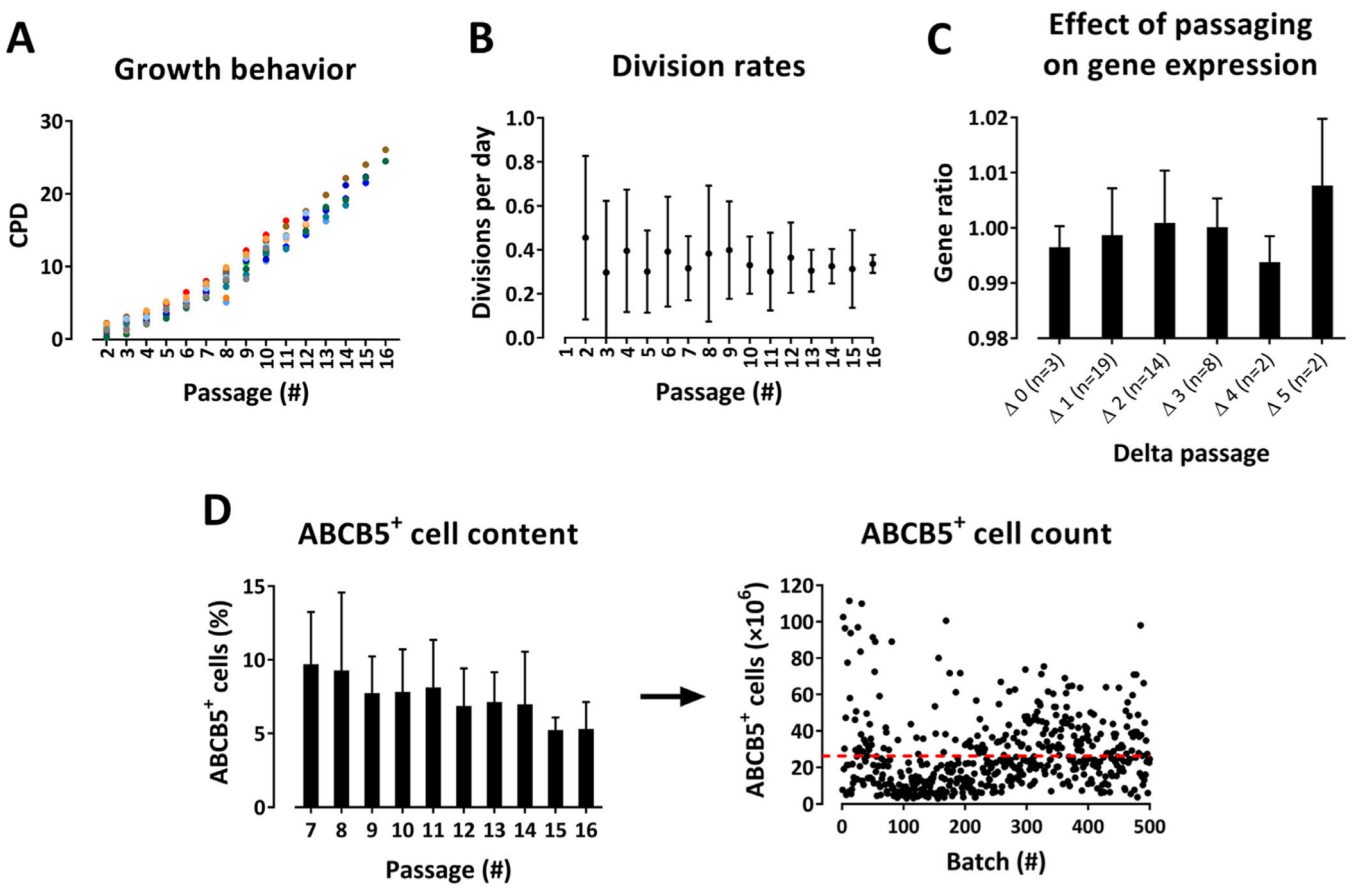

Figure 2.

Validation of the expansion process of ABCB5$^+$ MSCs. (A,B) Validation of passage number. Individual CPDs (n = 15 donors, represented by different colors) (A) and mean (± SD) division rates (n = 15 donors) (B), plotted against the respective passage number, demonstrating continuous cell expansion during up to 16 passages. (C) Comparability and homogeneity of batches between different passages of a given donor and between different donors as assessed by microarray-based gene expression analysis performed on samples from four various passages per donor for eight donors. Within each donor, the quantile-normalized data sets from the three higher passages were compared with the lowest passage. From each of these between-passage comparisons, the median gene ratio (of all genes that had shown an average signal >20 and at least 2-fold differential regulation) was determined. These values were used to calculate the median gene ratio (mean ± SD) for each delta passage value over all eight donors; n = number of between-passage comparisons with the delta passage value specified. Original microarray data were uploaded in Gene Expression Omnibus (accession no. GSE145589) and are available at https://www.ncbi.nlm.nih.gov/geo/query/acc.cgi?acc=GSE145589. (D) Relative amount (mean percentage ± SD) of ABCB5$^+$ cells in culture, plotted against the respective passage number (n = 17 donors) (left panel), and absolute yield of ABCB5$^+$ MSCs shown as single values from 500 batches derived from 260 donors, giving a mean count of 26.27×10^6 ABCB5$^+$ MSCs per batch (represented by red line, SD = 19.76×10^6) (right panel). SD, standard deviation. (Color version of figure is available online).

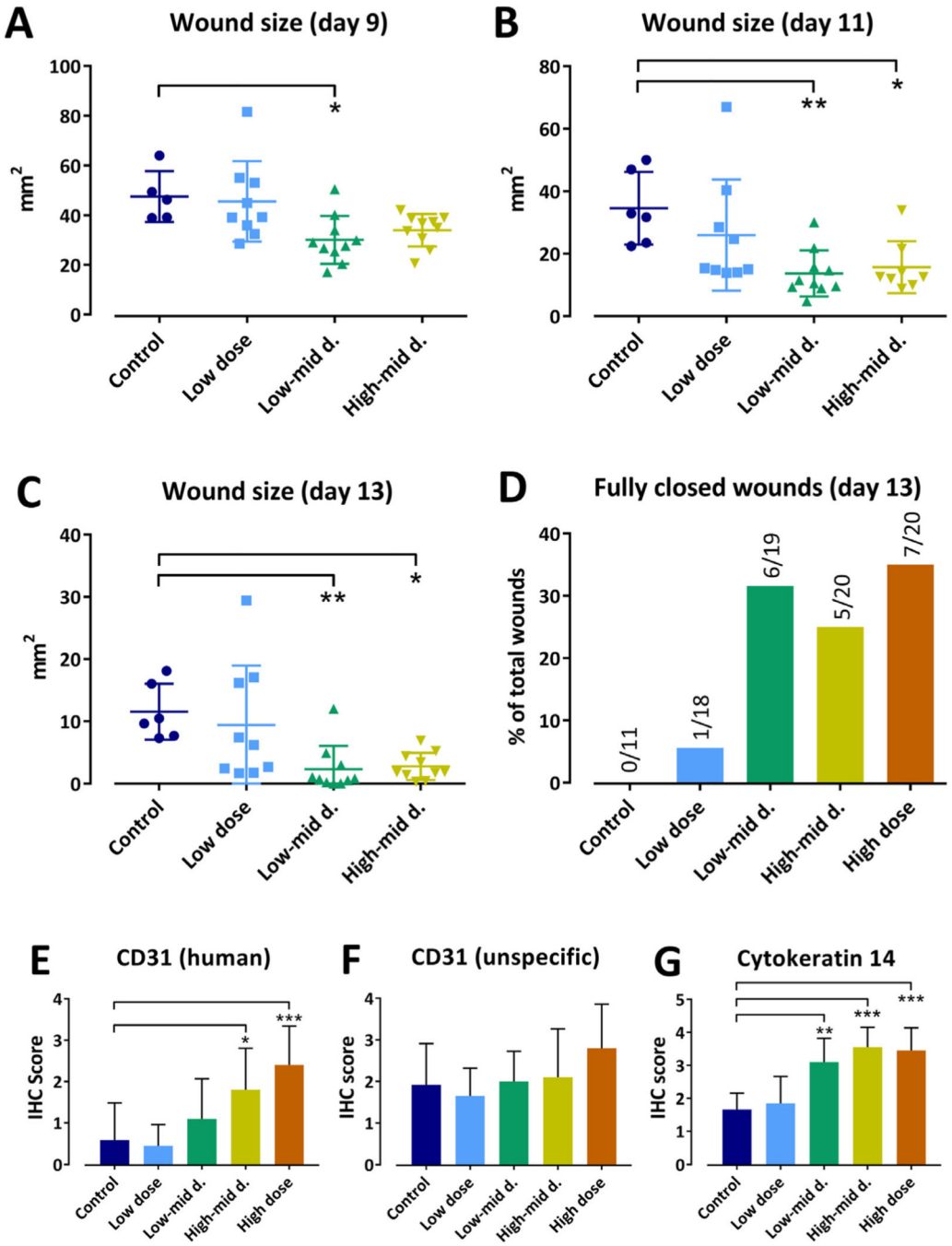

Figure 3.

Effect of topical application of ABCB5^{+} MSCs on healing of experimental full-thickness skin wounds in NSG mice. (A–C) Wound sizes (means of both wounds of each animal) at 9 days (A), 11 days (B) and 13 days (C) after vehicle (control) or MSC application. (D) Total number of fully closed wounds at 13 days after vehicle (control) or MSC application, shown as percentage value for each group. (E–G) Immunohistochemical evaluation of the wounds for human CD31 (E), unspecific CD31 (antibody-detected mouse and human CD31) (F) and cytokeratin 14 (G). Expression was semi-quantitatively quantified as no (−), slight (1+),

moderate (2+), strong (3+) and intense (4+) positivity. Shown are group means ± SD. Control: vehicle only (n = 12 wounds, six animals). Low dose: 1.875×10^5 $ABCB5^+$ MSCs per wound (n = 18 wounds, nine animals; one animal was prematurely euthanized). Low to mid dose: 3.75×10^5 $ABCB5^+$ MSCs per wound (n = 19 wounds, 10 animals; one wound was pathologically not evaluable). Mid to high: 7.5×10^5 $ABCB5^+$ MSCs per wound (n = 20 wounds, 10 animals). High dose: 1.5×10^6 $ABCB5^+$ MSCs per wound (n = 20 wounds, 10 animals). The high-dose group was excluded from wound size analysis (A–C) because of significantly smaller baseline wound size values (not shown). Non-parametric Kruskal-Wallis test followed by Dunn's multiple comparisons. $*P < 0.05$, $**P < 0.01$, $***P < 0.01$ versus control. d., dose; IHC, immunohistochemistry; SD, standard deviation. (Color version of figure is available online).

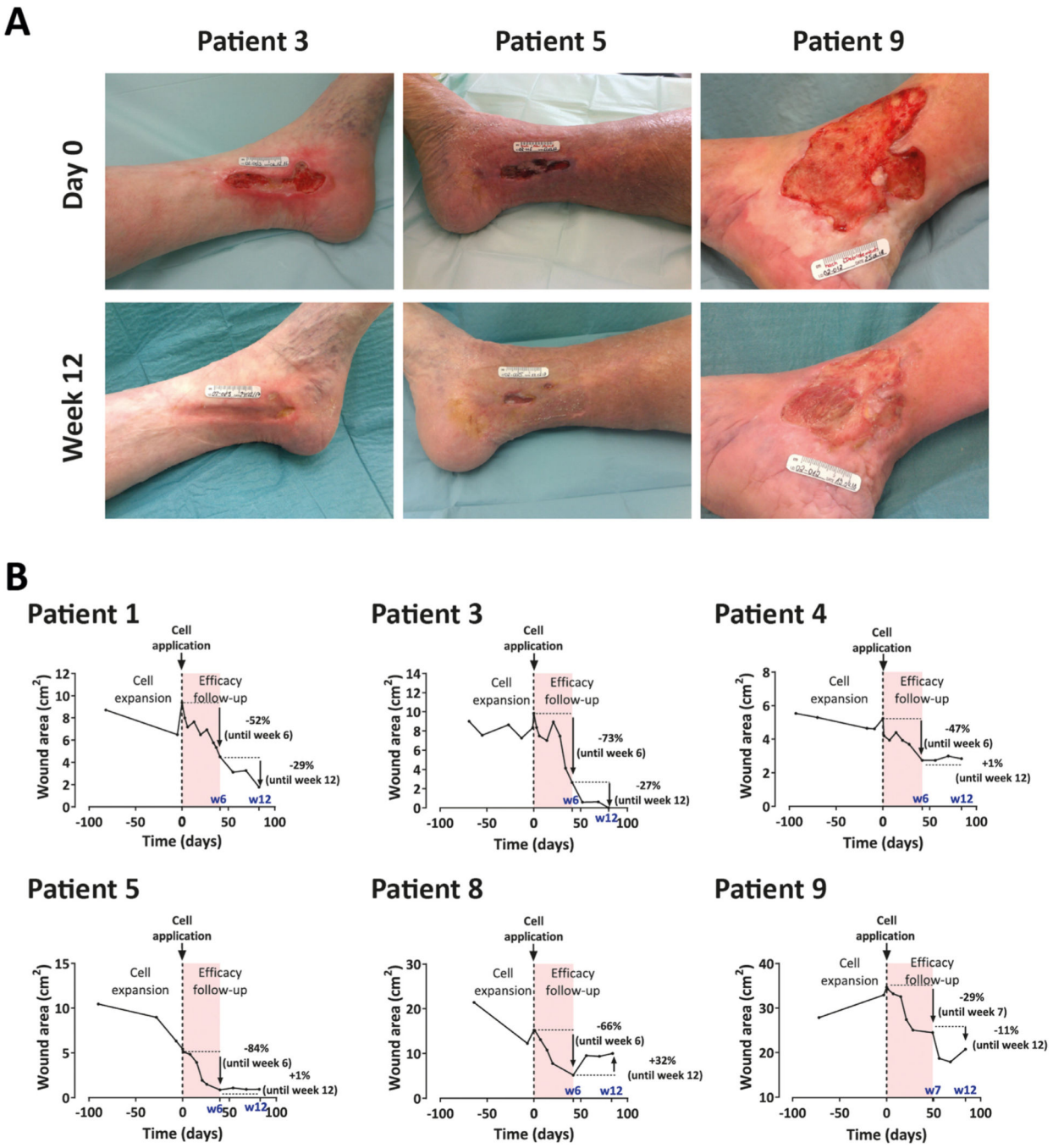

Figure 4.

Effect of topical application of 5×10^5 autologous skin-derived ABCB5$^+$ MSCs per cm^2 wound area on healing of human chronic venous ulcers. (A) Photographs of the target wounds of three representative patients before (day 0, upper panel) and 12 weeks after (lower panel) cell application. For photographs of all patients who were eligible for efficacy evaluation, see supplementary Figure 4. (B) Wound closure kinetics before (during cell expansion) and throughout the 12-week period following cell application (efficacy follow-up). Shown are all patients who were eligible for efficacy evaluation. For patient 8, wound

size data at week 4 are missing. Increase in the wound after week 6 coincided with two changes in routine wound care; namely, less frequent (once instead of twice weekly) dressing changes and a switch to less absorbent dressing (Mepilex instead of Biatain). For patient 9, wound size data at week 6 are missing; instead, week 7 measurement is included in the graph. Red shaded areas highlight the first 6 weeks of efficacy follow-up, during which wound healing was most pronounced. w6, week 6; w7, week 7; w12, week 12. (Color version of figure is available online).

Table 1

Specifications and results from routine batch analysis.

Parameter	n	Test method	Specification	Results
Microbiological control	155	BacT/ALERT system (adapted to 2.6.27 Ph. Eur.)	No growth	No growth in 99.35% of samples analyzed
Mycoplasma	155	Nucleic acid test-based assay (2.6.7 Ph. Eur.)	Not detectable (<10 CFU/mL)	Not detectable in 100% of samples analyzed
Endotoxin level	155	Limulus amebocyte lysate test (2.6.14 Ph. Eur.)	<2 EU/mL	<2 EU/mL in 100% of samples analyzed
Cell count	155	Flow cytometry (2.7.29 Ph. Eur.)	2.5 x 106to25 x 106 cells per cryovial	Within specified range
Cell vitality	155	Flow cytometry (2.7.29 Ph. Eur.)	>75%	98.27% § 1.01%[a]
Cell viability	155	Flow cytometry (2.7.29 Ph. Eur.)	>90%	99.1% § 1.1%[a]
CD90 expression	155	Flow cytometry	>90% CD90+ cells	98.48% § 3.3%[a]
Bead residues	155	Flow cytometry	<0.5%	0.03% § 0.03%[a]
ABCB5+ cell content	155	Flow cytometry	>90%	94.61% § 2.1%[a]
Angiogenic differentiation	155	Tube formation assay	Capillary structure formation	Capillary structure formation in 100% of samples analyzed
IL-lRAsecretion	75[b]	ELISA	>125 pg/mL	>125 pg/mL in 99.7% of samples analyzed

CFU, colony-forming units; ELISA, enzyme-linked immunosorbent assay; EU, endotoxin units; Ph. Eur., European Pharmacopoeia.

[a]Values are mean ± standard deviation.

[b]Historically, the IL-1RA secretion assay was implemented in the authors' regular test matrix at a later date, which is the reason for the lower sample number.